Multiobjective Model Predictive Control of LCL Grid-Connected Inverter Based on an Improved Gray Wolf Algorithm

Fengxiang Wang, *Senior Member, IEEE*, Feng Cai, Dongxiao Huang, *Senior Member, IEEE*, Yao Wei, *Member, IEEE*, Dongliang Ke, *Senior Member, IEEE*, and Zhenbin Zhang, *Senior Member, IEEE*

***Abstract*—To address the challenges of high-current harmonic distortion, excessive switching losses, and less desirable dynamic response in the single-phase LCL grid-connected inverter, this article proposes a multiobjective model predictive control (MOMPC) method based on an improved gray wolf optimization (IGWO) algorithm. The proposed method first establishes the mathematical model of the LCL inverter and formulates the cost function of FCS-MPC. Subsequently, the voltage of the capacitor is introduced to impose constraints on the cost function, thereby constructing the MOMPC to further enhance the control performance. Finally, the IGWO algorithm is employed to perform offline multiobjective optimization on current error, total harmonic distortion, and switching frequency to design the optimal weighting coefficients of MOMPC. In contrast to traditional MPC methods, the IGWO-based MOMPC can reduce total harmonic distortion, switching frequency, and control errors while enhancing system robustness and dynamic performance. The simulation and experimental results validate the feasibility and effectiveness of the proposed method.**

***Index Terms*—Finite control set model predictive control, improved gray wolf optimization (IGWO) algorithm, LCL grid-connected inverter, multiobjective control.**

Received 17 January 2025; revised 15 April 2025; accepted 14 May 2025. Date of publication 21 May 2025; date of current version 30 June 2025. This work was supported in part by the Science and Technology Program of Fujian Province under Grant 2024T3037 and Grant 2022HZ028010, in part by the Fujian Science & Technology Innovation Laboratory for Optoelectronic Information of China under Grant 2024CXY102, and in part by the Science and Technology Program of Quanzhou City under Grant 2023C002R. Recommended for publication by Associate Editor Gab-Su (SSGAE | OJ GAE) Seo. *(Corresponding author: Dongxiao Huang.)*

Fengxiang Wang, Dongxiao Huang, Yao Wei, and Dongliang Ke are with the Quanzhou Institute of Equipment Manufacturing, Haixi Institutes, Chinese Academy of Sciences, Jinjiang 362200, China, also with the Fujian Science and Technology Innovation Laboratory for Optoelectronic Information of China, Fuzhou 350108, China, and also with the Fujian Institute of Research on the Structure of Matter, Chinese Academy of Sciences, Fuzhou 350025, China (e-mail: fengxiang.wang@fjirsm.ac.cn; dongxiao.huang@fjirsm.ac.cn; yao.wei@fjirsm.ac.cn; dongliang.ke@fjirsm.ac.cn).

Feng Cai is with the College of Mechanical and Electrical Engineering, Fujian Agriculture and Forestry University, Fuzhou 350100, China, and also with the Quanzhou Institute of Equipment Manufacturing, Haixi Institutes, Chinese Academy of Sciences, Jinjiang 362200, China (e-mail: 5221239025@fafu.edu.cn).

Zhenbin Zhang is with the School of Electrical Engineering, Shandong University, Jinan 250061, China (e-mail: zbz@sdu.edu.cn).

Color versions of one or more figures in this article are available at https://doi.org/10.1109/TPEL.2025.3572213.

Digital Object Identifier 10.1109/TPEL.2025.3572213

NOMENCLATURE

Parameter	*Description*
V_{dc}	DC side voltage.
C_{dc}	DC capacitance.
L_1, L_2	Filter inductors.
C	Filter capacitor.
R_1, R_2	Internal resistances of inductors L_1 and L_2
R_c	Internal resistance of capacitance C
v_g	Grid-connected voltage.
U_{ab}	Output voltage at the midpoint of the bridge leg.
i_1, i_g	Currents flowing through inductors L_1 and L_2
i_c	Current flowing through Filter capacitor.
λ_x, λ_y, λ_z	Weighting coefficients.
x_{ref}, y_{ref}, z_{ref}	Reference values.
a, b, c	Weighting coefficients.
LCL	Inductor–capacitor–inductor.
PI	Proportional–integral.
MPC	Model predictive control.
FCS-MPC	Finite control set model predictive control.
MOMPC	Multiobjective model predictive control.
PWM	Pulsewidth modulation.
THD	Total harmonic distortion.
GWO	Gray wolf optimization.
PSO	Particle swarm optimization.
WOA	Whale optimization algorithm.
IGWO	Improved gray wolf optimization.
GA	Genetic algorithm.
SOGI	Second-order generalized integrator.
PLL	Phase-locked loop.
ITAE	Integral of the time-weighted absolute error.
Std	Standard deviation.

I. INTRODUCTION

IN RECENT years, with the widespread adoption of renewable energy and the rapid development of smart grid technology, the LCL-type grid-connected inverter has become a crucial component in renewable energy integration due to its superior filtering performance and high power density [1], [2]. However, increasing grid complexity and the inherent variability of renewable energy sources pose significant challenges to inverter control strategies. Regulatory effective inverter output

TABLE I
FCS-MPC BASIC OBJECTIVE FUNCTION

Control variable	Application scenario	Objective function
Current	Predictive current control	$g_i = \lvert i_{\text{ref}} - i\rvert^2$
Voltage	UPS voltage predictive control	$g_v = \lvert v_{\text{ref}} - v\rvert^2$
Active power	Converter, motor control	$g_P = \lvert P_{\text{ref}} - P\rvert$
Reactive power	Converter, motor control	$g_Q = \lvert Q_{\text{ref}} - Q\rvert$
Torque	Motor control	$g_T = \lvert T_{\text{eref}} - T_e\rvert$
Magnetic chain	Motor control	$g_\psi = \lVert\psi\rVert_{\text{ref}} - \lvert\psi\rvert$

current to ensure power quality and system stability has become a focal point of research [3], [4].

Existing control schemes for grid-connected inverters exhibit various limitations. While hysteresis control is relatively straightforward, it is plagued by issues such as high switching frequency and low-frequency harmonics, ultimately resulting in degraded power quality. Despite its widespread use due to its simplicity, PI control exhibits limited dynamic response and is highly sensitive to variations in parameters. Repetitive control offers high accuracy but responds slowly to disturbances, while sliding mode control ensures robustness but is prone to chattering and requires an appropriately designed sliding trajectory.

MPC has emerged as an advanced model-based control method that dynamically optimizes control input by predicting future system behavior in real time while considering system constraints [5]. Among its variants, FCS-MPC has gained significant attention in power electronic applications due to its ability to directly apply control actions to power converters without requiring a PWM modulator. This characteristic makes FCS-MPC inherently simple and flexible in design. Moreover, its cost function enables the integration of multiple constraints, facilitating multiobjective cooperative control [6].

In complex power systems, simultaneous optimization of multiple performance indicators, such as inverter output current THD, switching frequency, and dynamic response speed,is critical to maintaining system efficiency, stability, and power quality [7]. The flexibility of FCS-MPC to incorporate various objectives into its cost function makes it well suited for such scenarios [8]. It can control typical variables such as current, voltage, torque, or magnetic flux while simultaneously meeting additional requirements such as reducing switching frequency, mitigating common-mode voltage, and regulating reactive power [9].

However, conventional FCS-MPC methods are typically designed to optimize single objectives, such as output current or voltage control, as summarized in Table I [10]. This single-objective focus limits their ability to address the diverse and often conflicting performance requirements of complex systems. Moreover, parameter optimization in these traditional methods is computationally intensive and time-consuming, further restricting their applicability in real-time or large-scale systems [11].

To address these limitations, MOMPC has been developed. By framing the control problem as a multiobjective optimization task, MOMPC enables real-time strategy optimization that balances various performance metrics. This approach not only fulfills the overall performance needs of the system, but also ensures comprehensive consideration of multiple objectives, paving the way for improved control in complex power systems.

However, the complexity of multiobjective optimization problems and the mutual conflicts between different objectives make the design and implementation of MOMPC challenging [12]. Among them, the selection of the weighting coefficients is not a simple problem for several reasons. On the one hand, even though FCS-MPC has been successfully used in practical applications for several years, it still lacks theoretical analyses compared to other MPC techniques, and in recent years this problem has been gradually being solved. However, the value of the weighting coefficients affects the performance of the system and the weighting coefficients are not fixed, so it is necessary to choose appropriate values for the system.

Multiobjective predictive control commonly adopts the weighting coefficient method to balance and prioritize multiple objectives. In this approach, each objective in the cost function is assigned a weighting coefficient, which adjusts the relative importance of the objectives based on the control requirements. The configuration of these coefficients significantly impacts system performance and stability. However, due to the inherent interactions between multiple control objectives, altering the weight of one objective can degrade the performance of others [13]. Moreover, since the importance and magnitude of each objective often vary greatly, the overall system performance is not a straightforward summation, making the determination of the appropriate weighting coefficients a complex task [14].

Currently, there are no standardized methods or universal guidelines for configuring weighting coefficients. Most approaches rely on empirical knowledge or trial-and-error methods. A typical strategy is to fix the weighting coefficient of the primary control objective at 1, gradually increase the coefficients of secondary objectives from 0, and iteratively evaluate the performance of the system. This process is repeated until all performance requirements are met. However, such methods are labor-intensive and require extensive experimentation, calculations, and repeated adjustments. This complexity highlights the need for an algorithm capable of ensuring system stability while efficiently optimizing the weighting coefficients, thereby improving the efficiency and reliability of MOMPC.

Patricio Cortés used system debugging to investigate changes and derive the relationship between the weighting coefficients and the system [15]. This method provides an intuitive way to understand the relationship between the weighting factors and the behavior of the system. However, it relies heavily on manual tuning and system-specific experimentation, which makes it time consuming and less adaptable to varying conditions.

PSO is simple and fast and has been used to design the parameters in the drive system [16], [17]. Its main advantages are its simplicity and fast convergence, making it computationally efficient. However, PSO is prone to premature convergence and may struggle with complex, multimodal objective functions, limiting its ability to find truly optimal solutions in some scenarios. As a more advanced GA, the nondominated sorting genetic algorithm II has been applied in the field design of FCS-MPC weighting factors. However, the coding/decoding process of GA increases its complexity and limits its ability to deal with nonlinear constraints [18], [19].

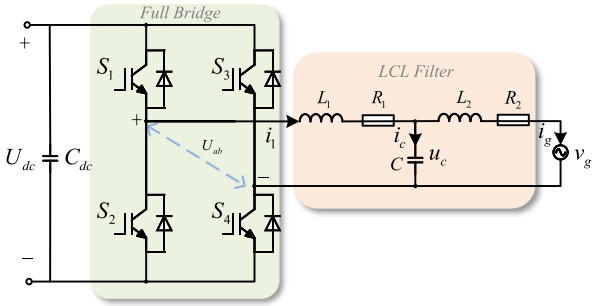

Fig. 1. Topology of single-phase LCL grid-connected inverter.

In [20], a data-driven online learning controller was proposed to enhance the system performance. In [21], this approach was simplified by optimizing a single weighting factor in the MPC algorithm. However, both methods face challenges in adapting to rapid dynamic changes due to the low convergence rates inherent in their online optimization processes. In addition, the online adjustment of controller parameters significantly increases computational cost, resulting in higher processing delays.

GWO is a swarm intelligence optimization method inspired by the natural hunting behavior of gray wolves. It exhibits a strong global search capability and good convergence performance [22]. Nevertheless, standard GWO can suffer from slow exploitation in later stages, reducing fine-tuning precision and potentially affecting the final optimization results.

In order to effectively solve these problems, this article proposes an MOMPC strategy based on the improved gray wolf optimization (IGWO) algorithm. By combining IGWO with MOMPC, effective optimization of the control parameters of LCL grid-connected inverters can be achieved, taking into account multiple performance objectives and improving the comprehensive control performance of the system. The major contributions of this article are as follows.

1) An MOMPC strategy based on the IGWO algorithm is proposed for the single-phase LCL-type inverters to enhance control accuracy and current quality.
2) A hybrid IGWO algorithm is designed to improve search precision and global optimization capability.
3) The proposed control strategy is evaluated through simulations and experiments, demonstrating its effectiveness and advantages.

The rest of this article is organized as follows. Section II describes the modeling of the single-phase LCL-type inverter; Section III is a study of the MOMPC strategy and the process of IGWO; Section IV presents the simulation results of the algorithm's test runs; Section V shows the results of the experimental tests carried out on the system. Finally, Section VI concludes this article.

II. LCL Grid-Connected Inverter Mathematical Model

Fig. 1 shows the main circuit topology of the LCL grid-connected inverter. It is composed of a full-bridge inverter, inductance L_1 on the inverter side, filter capacitor C, inductance L_2 on the net side and parasitic resistance, among which L_1, L_2, and C constitute the LCL filter.

TABLE II
Output Voltage of Single Phase Inverter for Four Possible Switching States

Switching vector	S1	S2	S3	S4	S	Output voltage
1	1	0	0	1	1	U_{dc}
2	1	0	1	0	0	0
3	0	1	1	0	-1	$-U_{\mathrm{dc}}$
4	0	1	0	1	0	0

According to Kirchhoff's law, the system can be represented as follows:

$$\begin{cases} L_1 \frac{di_1}{dt} + R_1 i_1 = U_i - u_c \\ L_2 \frac{di_g}{dt} + R_2 i_g = U_c - v_g \\ C \frac{dU_c}{dt} = i_1 - i_g \end{cases} \tag{1}$$

where $U_i = U_{ab}$. Considering two gate signals of power switches, which can take values of 1 or 0 on behalf of the ON or OFF state, there is a total of four different switching states. Define $S = S_1 \cdot S_4 - S_2 \cdot S_3$ as the total switching function of the inverter, and the switching function of the inverter is shown in Table II below [23].

Based on (1), a discrete-time predictive model for i_1 is obtained using the forward Euler method at T_s [24]

$$i_1(k+1) = \left(1 - \frac{T_s}{L_1} R_1\right) i_1(k) + \frac{T_s}{L_1} \left[U_i(k) - u_c(k)\right] \tag{2}$$

where $U_i = U_{ab} = S \cdot U_{dc}$, which can be step-changed by changing the four switching states.

To select the optimal vector that can obtain the least error between the reference and predicted currents, the cost function should be established to reflect the difference between the predicted and reference currents. Therefore, in terms of the absolute error, the cost function can be expressed as

$$g = \left|i_1^*(k+1) - i_1(k+1)\right|^2 \tag{3}$$

where the reference i_1^* is calculated by the given reference i_g^* described as follows. If i_g^* were given by the grid voltage u_g and a coefficient K: $i_g^* = K v_g = K v_g \sin(\omega t)$, the reference u_c^* would be obtained by inserting the expressions of i_g^* and u_g into (1)

$$u_c^* = v_g \left[(1 + KR_2)\sin(\omega t) + \omega K L_2 \cos(\omega t)\right] \tag{4}$$

where ω is the fundamental angular frequency of the grid voltage. Then, the expression of i_1^* could be obtained by substituting (4) and i_g^* into (1)

$$i_1^* = v_g \left[K(1 - \omega^2 C L_2)\sin(\omega t) + \omega C(1 + KR_2)\cos(\omega t)\right]. \tag{5}$$

III. Proposed IGWO-Based MOMPC

Fig. 2 illustrates the control block diagram of the LCL grid-connected inverter. The system employs a dual-loop control

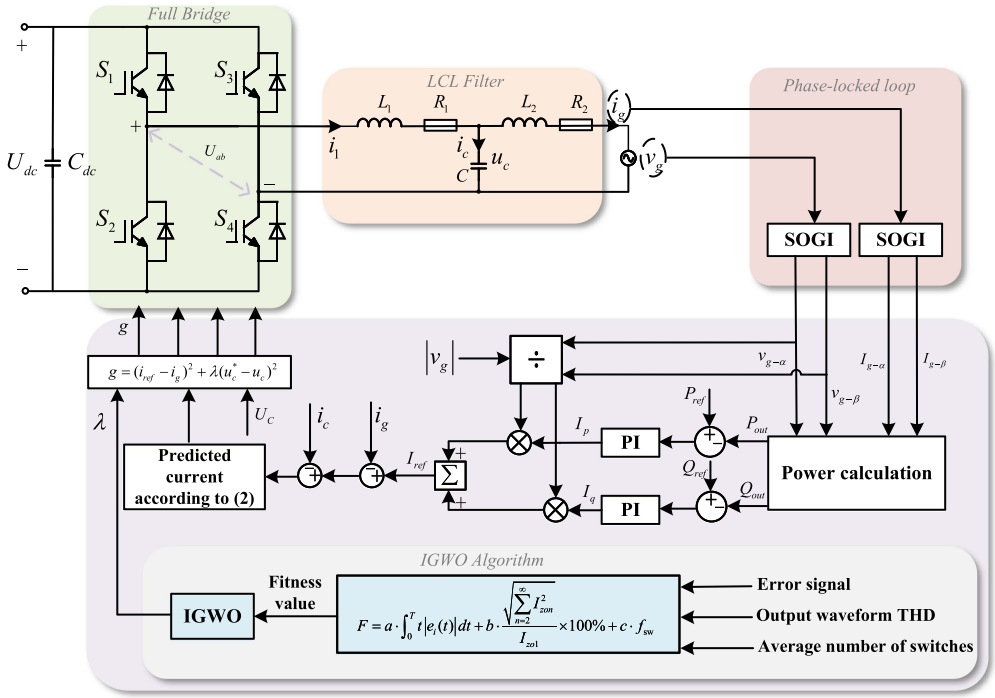

Fig. 2. Control block diagram of the proposed IGWO-MOMPC strategy.

strategy comprising an outer power loop and an inner current loop with active damping. Typically, the reactive power reference is set to zero. The active power reference is specified by the user or determined on the basis of the instantaneous output power requirements of the system. In photovoltaic applications, the active power reference corresponds to the maximum power point, as determined by the maximum power point tracking algorithm.

The controller is designed to calculate the instantaneous active and reactive power using the two quadrature signals generated by the SOGI as follows:

$$P = \frac{1}{2}\left(v_{g-\alpha} \cdot I_{g-\alpha} + v_{g-\beta} \cdot I_{g-\beta}\right) \tag{6}$$

$$Q = \frac{1}{2}\left(v_{g-\beta} \cdot I_{g-\alpha} - v_{g-\alpha} \cdot I_{g-\beta}\right). \tag{7}$$

By comparing them with the corresponding reference values, the sum is obtained and multiplied by the two sinusoidal signals generated by the SOGI to obtain the grid current reference signal I_{ref} as follows:

$$I_{\text{ref}} = I'_p + I'_q = \frac{I_p v_{g-\alpha} + I_q v_{g-\beta}}{|v_g|}. \tag{8}$$

This represents the reference current I_{ref}, calculated as the sum of the components I'_p and I'_q, where I_p and I_q are weighted by the grid voltages $v_{g-\alpha}$ and $v_{g-\beta}$, normalized by the magnitude of the grid voltage $|v_g|$.

A. Multiobjective Model Predictive Control

A single control objective cannot meet the demand, in which case the objective function of multiple control objectives must be considered. MPC can integrate unify multiple control objectives into a single objective function to optimize overall system performance [25], whose objective function formula is usually shown as follows:

$$g = \lambda_x(x_{\text{ref}} - x)^2 + \lambda_y(y_{\text{ref}} - y)^2 + \cdots + \lambda_z(z_{\text{ref}} - z)^2 \tag{9}$$

where x, y and z are predicted values.

The control objective of the grid-connected inverter studied in this article is the output current, for which there are two requirements: 1) the error between the output current and the reference current is as small as possible; 2) the waveform of the output current is as smooth as possible, with a small THD value. The first requirement ensures the basic shape of the output current as the main control objective; the second requirement is to be able to suppress the fluctuation of the output current as the secondary control objective. The error can be expressed as the square of the difference between the reference current and the output current, that is $(i_{\text{ref}} - i_g)^2$; while the smoothness of the output current is affected by the control quantity u_c, the error that can be used by u_c to suppress the fluctuation of the current. Combining the primary and secondary control objectives, the cost function is constructed, as shown in the following:

$$g = (i_{\text{ref}} - i_g)^2 + \lambda(u_c^* - u_c)^2 \tag{10}$$

where λ is the weight coefficient. From (10), it can be seen that the cost function consists of two parts. The first part is the sum of the squared differences between the reference and actual values of the inverter output current. This term reflects the quality of the inverter output current: the smaller its value, the smaller the error between the output and reference currents, leading to better

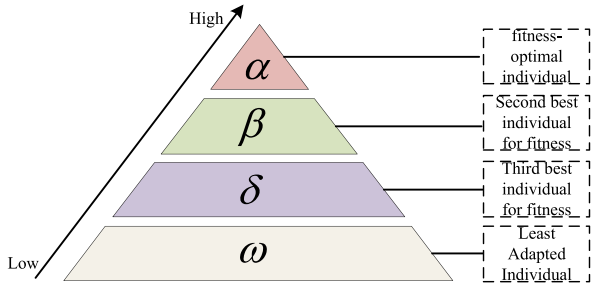

Fig. 3. Schematic of gray wolf population classes.

power quality. The second is the sum of the squares of the errors between the inverter capacitor output voltage and the reference voltage, which indirectly controls the waveform of the current and suppresses the capacitor voltage error, thus achieving the control of the current. λ is used to adjust the importance of the capacitor voltage in the cost function, its value should not be too large or too small, too large will cause an inconsistency between the predicted behavior and the reference value, and too small will not achieve the objective of improving the THD of the system.

B. Optimization Method

To ensure that the current waveform on the grid side meets the grid connection requirements and can quickly track changes in the reference current, the objective function for the inverter control parameters in the grid-connected mode is designed to include three weighted terms: the ITAE, the THD of the grid current, and the number of switching actions of the power switches [26]

$$F = a \cdot \int_0^T t\,|e_i(t)|\,dt + b \cdot \frac{\sqrt{\sum_{n=2}^{\infty} I_{zon}^2}}{I_{zo1}} \times 100\% + c \cdot f_{\text{sw}} \tag{11}$$

where $a + b + c = 1$. The term $e_i(t)$ represents the error between the generated reference value and the feedback value of the power loop, while f_{sw} denotes the average number of switching events. By adjusting the values of a, b, and c, the performance of the system can be tailored to meet different requirements, ensuring a low harmonic distortion rate in the current connected to the grid while maintaining a fast dynamic response.

The core concept of the GWO algorithm is to simulate the social hierarchy and hunting behavior of gray wolves to iteratively search for the optimal solution. As apex predators, gray wolves usually live and hunt in packs, with a population size that generally ranges from 5 to 12 wolves [27]. The gray wolf population follows a strict social hierarchy, as shown in Fig. 3.

In the GWO algorithm, the hierarchy of wolves plays a crucial role. The α wolf, recognized as the most intelligent and capable, is primarily responsible for decision-making during hunting (merit-seeking) and general pack management [28]. The β wolf, second in command, assists the α wolf in decision-making and assumes leadership when necessary [29]. The δ wolves, positioned lower in the hierarchy, support the α and β wolves by maintaining internal balance within the pack and caring for the young wolves.

Traditional GWO algorithm has been widely applied in fields, such as function optimization, neural networks, and image processing due to its flexibility and minimal parameter tuning requirements. In addition, it does not depend on the gradient information of the problem. However, it suffers from several drawbacks as follows.

1) Low convergence accuracy.
2) Insufficient stability.
3) Susceptibility to local optima.

To address these issues, this article proposes a hybrid IGWO algorithm with the following enhancements.

1) Improved population initialization: Using the good point set theory to enhance initialization quality and convergence efficiency.
2) Nonlinear convergence factor: Balancing global exploration and local exploitation using a nonlinear convergence adjustment strategy.
3) Enhanced search capability: Gaussian mutation and a greedy selection strategy are incorporated to prevent premature convergence and improve solution accuracy.

The IGWO algorithm is used to optimize the membership function process, as shown in Fig. 4. The fundamental steps of the optimization process are as follows.

Step 1: Define the dimension G of the gray wolf population, the population size N, and maximum iteration number $T_{\max}$.

Step 2: Generate the initial population individuals using the good point set theory. The principle is as follows: Let G_d be the unit cube in d-dimensional Euclidean space. If $r \in G_d$, then it is constructed as follows:

$$p_n(k) = \begin{cases} \{r_1(n) \times k\}, \{r_2(n) \times k\}, \ldots, \{r_d(n) \times k\} \\ 1 \le k \le n. \end{cases} \tag{12}$$

Its deviation satisfies the formula

$$\varphi(n) = C(r, \varepsilon) n^{-1+\varepsilon} \tag{13}$$

where $C(r, \varepsilon)$ is a constant that depends only on r and ε, where ε is an arbitrary positive number; $p_n(k)$ represents the good point set; r is a good point.

Step 3: Evaluate the fitness of each gray wolf using the objective function. Select the three wolves with the lowest value as α, β, and δ. Update the positions of the remaining ω wolves based on the positions of α, β, and δ, according to (14)–(17)

$$A = 2a \cdot r_1 - a \tag{14}$$

$$C = 2 \cdot r_2 \tag{15}$$

$$D_{\text{GWO}} = \left| C \cdot X_p(t) - X(t) \right| \tag{16}$$

$$X(t+1) = X_p(t) - A \cdot D \tag{17}$$

where $a = 2 - 2[(e^{t/t_{\max}} - 1)/(e - 1)]^k$, $k = 1.5$, r_1, r_2 are two random numbers generated using the good point set theory, D is the distance between an individual in the population and the prey (target), t is the number of iterations, $X(t+1)$ denotes the position of the individual in the t + 1st iteration.

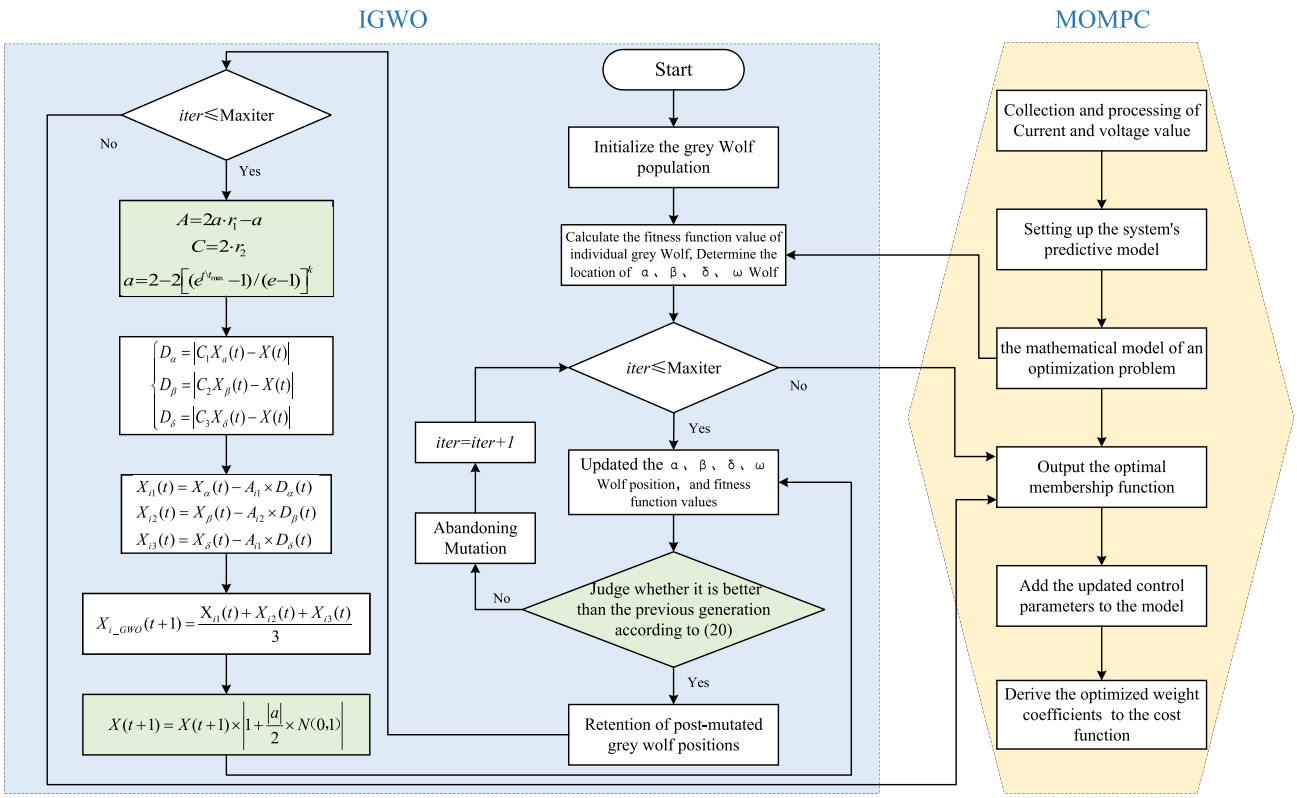

Fig. 4. Schematic diagram of the optimization process.

Step 4: Sort the wolves' individuals for fitness to get the best individual, perform a local adaptive search on the best individual's position, calculate the fitness and compare it with the optimal value, and select the solution with good fitness as the new optimal individual.

Step 5: Record the three positions of the gray wolf with the best fitness values in the first five steps as X_α, X_β, and X_δ. The first candidate for the new position of wolf $X_i(t)$ named $X_{i-\mathrm{GWO}}(t+1)$ is calculated as follows:

$$X_{i-\mathrm{GWO}}(t+1)=\frac{X_{i1}(t)+X_{i2}(t)+X_{i3}(t)}{3}. \tag{18}$$

Step 6: Generate new solutions around the optimal solution using random perturbations based on a standard Gaussian distribution. This enhances the algorithm's ability to explore a more diverse solution space and helps avoid local optima. The position update formula of the GWO algorithm after introducing the Gaussian mutation strategy is given as follows:

$$X(t+1)=X(t+1)\times\left|1+\frac{|a|}{2}\times N(0,1)\right| \tag{19}$$

where $N(0,1)$ denotes the standard Gaussian distribution.

Step 7: Incorporate the greedy selection strategy by comparing the fitness values of the mutated solution and the previous generation. If the fitness value of the best-mutated solution is superior to that of the original position, the mutated position is accepted as the final position for the current iteration. Otherwise, the original position remains unchanged to ensure stability in the solution. The formula is shown in

$$X_{\mathrm{best}}(t)=\begin{cases}X_{i,j}^{t+1}, & f(X_{i,j}^{t+1})<f(X_{\mathrm{best}}(t))\\ X_2(t), & f(X_{i,j}^{t+1})\geq f(X_{\mathrm{best}}(t))\end{cases} \tag{20}$$

where X_{best} represents the optimal solution.

Step 8: after performing this procedure for all individuals, the counter of iterations is increased by one, and the search can be iterated until the predefined number of iterations is reached. if not, return to Step 3, and if so, end the algorithm to output the control parameters.

IV. Simulation Results

To verify the effectiveness and superiority of the IGWO algorithm, this article conducts a comparative experimental analysis using PSO, WOA, and GWO. Eight commonly used single-peak and multipeak benchmark test functions are selected for evaluation. The population size of each algorithm is set accordingly, with a search space dimension of Dim = 30 and a maximum of 500 iterations. The core parameters of each algorithm, determined based on experimental requirements and algorithmic performance, are provided in Table III.

In order to verify the performance of the IGWO proposed in the previous section, eight commonly used single-peak and multipeak benchmark functions are selected for simulation testing. Among them are f_1-f_4 single-peak benchmark functions, as shown in Table IV, which have only a unique global optimal solution in the definition domain, and are suitable for evaluating

TABLE III
ALGORITHM PARAMETER SETTINGS

Algorithm	Parameter	Value
PSO	Acceleration factor (c_1)	2
	Acceleration factor (c_2)	2
GWO	Inertia weight (ω)	0.9
	Convergence factor a	Linearly decreases from 2 to 0
WOA	Spiral constant (b)	1
	A	Linearly decreases from 2 to 0
IGWO	Nonlinear adjustment coefficient k	1.5
	Convergence factor a	Linearly decreases from 2 to 0

TABLE IV
SINGLE-PEAK BENCHMARK FUNCTIONS

Name	Benchmark function	Dim	Range	$f_{\min}$
Sphere	$f_1(x)=\sum_{i=1}^{n}x_i^2$	30	$x_i\in[-100,100]$	0
Rosenbrock	$f_2(x)=\sum_{i=1}^{n-1}\left[100(x_{i+1}-x_i^2)^2+(x_i-1)^2\right]$	30	$x_i\in[-30,30]$	0
Quartic	$f_3(x)=\sum_{i=1}^{n}ix_i^4+\text{random}(0,1)$	30	$x_i\in[-1.28,1.28]$	0
Schwefel	$f_4(x)=\sum_{i=1}^{30}\lvert x_i\rvert+\prod_{i=1}^{30}\lvert x_i\rvert$	30	$x_i\in[-10,10]$	0

TABLE V
MULTIPEAK BENCHMARK FUNCTIONS

Name	Benchmark function	Dim	Range	$f_{\min}$
Girewank	$f_4(x)=\sum_{i=1}^{n}\frac{x_i^2}{4000}-\prod_{i=1}^{n}\cos\left(\frac{x_i}{\sqrt{i}}\right)+1$	30	$x_i\in[-600,600]$	0
Rastrigin	$f_5(x)=\sum_{i=1}^{n}\left[x_i^2-10\cos(2\pi x_i)+10\right]$	30	$x_i\in[-5.12,5.12]$	0
Ackley	$f_6(x)=-20\exp\left(-0.2\sqrt{\frac{1}{n}\sum_{i=1}^{n}x_i^2}\right)-\exp\left(\frac{1}{n}\sum_{i=1}^{n}\cos(2\pi x_i)\right)+20+e$	30	$x_i\in[-32,32]$	0
Schafer	$f_7(x)=0.5+\frac{\sin^2\left(\sqrt{x_1^2+x_2^2}\right)-0.5}{(1+0.001(x_1^2+x_2^2))^2}$	30	$x_i\in[-100,100]$	0

the local optimization efficiency and convergence speed of the IGWO algorithm; and f_5-f_8 are multipeak benchmark functions, as shown in Table V, which have multiple local extreme points in the definition domain, and can effectively test the algorithm's global exploratory ability and the characteristics of avoiding premature convergence. In Tables IV and V, Dim is the spatial dimension of the test function, indicating the number of independent variables in the function; Range defines the domain of the function, representing the optimization interval; $f_{\min}$ denotes the theoretical optimal value of the test function.

Due to the inherent stochastic nature of population-based optimization algorithms, each test function was independently executed 30 times to minimize the impact of randomness and improve the reliability of the results. The simulation results are presented in Tables IV and V. The convergence accuracy and speed of the algorithm were assessed using the Mean, while Std was used to measure the dispersion of the solutions, reflecting the stability of the algorithm.

The single-peak function is generally used to test the convergence speed of the algorithms. In this study, under the same spatial dimension and search range, the four optimization algorithms were tested using the single-peak functions listed in Table IV, with the results summarized in Table VI. The results indicate that, for the functions f_1, f_3, and f_4, the IGWO algorithm significantly outperforms the other three algorithms in all optimization metrics, achieving the best performance. Although IGWO did not exceed WOA in optimizing f_2, the difference in results was minimal, demonstrating the strong precision and stability of the IGWO solution.

Furthermore, four commonly used multipeak functions shown in Table V were used to evaluate the four optimization algorithms under the same spatial dimension and search range. The results for f_5–f_8 are summarized in Table VII. Multipeak functions are typically used to test the global search capability of algorithms. As seen in Table VII, IGWO outperforms the other algorithms in

TABLE VI
SIMULATION RESULTS OF SINGLE-PEAK TEST FUNCTION

Benchmark functions	Result	Algorithm PSO	WOA	GWO	IGWO	Rank
f_1	Best	12.2571	2.1509E-24	1.1777	0	1
	Worst	42.0716	2.2293E-19	38.8397	0	
	Mean	24.8028	1.7143E-20	11.7611	0	
	Std	8.3019	4.5161E-20	9.7226	0	
f_2	Best	287.9664	26.8052	86.706	28.7806	2
	Worst	3719.3621	28.7317	2963.4462	30.8356	
	Mean	1147.0061	27.8878	673.5711	29.7962	
	Std	839.5822	0.48491	763.3119	0.5789	
f_3	Best	0.018756	0.00059189	0.0019294	0.0012424	1
	Worst	0.18879	0.05542	0.23354	0.045624	
	Mean	0.0060406	0.012764	0.080096	0.013789	
	Std	0.031301	0.011479	0.044213	0.0099754	
f_4	Best	2.6189	9.0584E-17	0.33203	1.0453E-21	1
	Worst	14.5054	6.3508E-13	8.9486	5.7326E-15	
	Mean	5.2829	6.5536E-14	1.204	2.3086E-16	
	Std	2.3471	1.4693E-13	1.5039	1.0434E-15	

TABLE VII
SIMULATION RESULTS OF MULTIPEAK TEST FUNCTION

Benchmark functions	Result	Algorithm PSO	WOA	GWO	IGWO	Rank
f_5	Best	1.076	0	0.96251	0	1
	Worst	1.4829	0.47812	1.4749	0.11073	
	Mean	1.2372	0.050805	1.0931	0.0078274	
	Std	0.1027	0.13575	0.10488	0.025468	
f_6	Best	28.5446	0	16.5593	0	2
	Worst	80.2909	1.7764E-15	127.7901	0	
	Mean	48.9122	5.9212E-17	62.5503	0	
	Std	13.3107	3.2432E-16	28	0	
f_7	Best	2.986	4.44-0E-16	0.56329	0	1
	Worst	6.6809	7.5495E-15	3.3506	0	
	Mean	4.907	4.8258E-15	2.0076	0	
	Std	0.75035	2.412E-15	0.6397	0	
f_8	Best	0.13292	0	0.032838	0	1
	Worst	0.2898	0.0062242	0.49832	0	
	Mean	0.2135	0.0024993	0.47162	0	
	Std	0.036823	0.001718	0.03585	0	

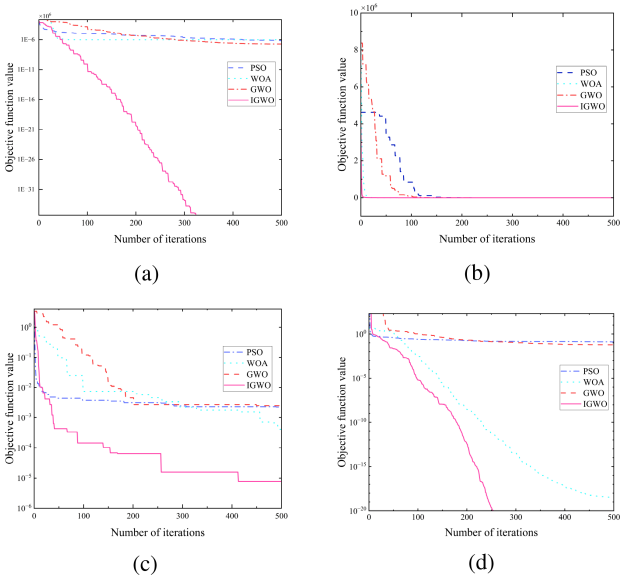

Fig. 5. Convergence curve of single-peak test function. (a) Convergence curve for f_1 adaptation. (b) Convergence curve for f_2 adaptation. (c) Convergence curve for f_3 adaptation. (d) Convergence curve for f_4 adaptation.

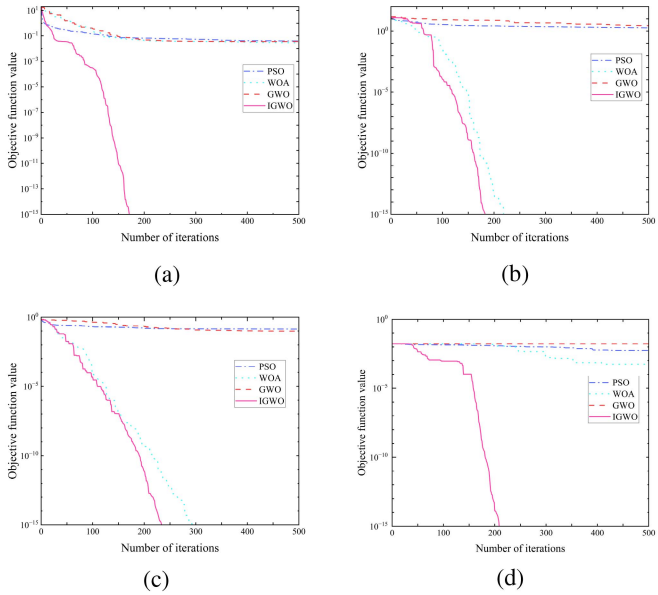

Fig. 6. Convergence curve of multipeak test function. (a) Convergence curve for f_5 adaptation. (b) Convergence curve for f_6 adaptation. (c) Convergence curve for f_7 adaptation. (d) Convergence curve for f_8 adaptation.

optimizing all four high-dimensional multipeak test functions, successfully finding the optimal solution in all cases except f_5 in 30 independent tests. Although the optimal precision for f_5 reached 0, its standard deviation was slightly above the ideal value of 0 but remained close to the optimal level. A comprehensive analysis of the four optimization algorithms indicates that IGWO has the lowest standard deviation, demonstrating not only high convergence accuracy, but also strong stability in diverse test environments. This further validates the superiority of IGWO in solving complex high-dimensional multipeak optimization problems.

In the analysis of the optimization results of single-peak and multipeak test functions, this article selects the convergence curves of the optimization fitness values of 30 independent runs and calculates their statistical means to assess the convergence speed and optimization finding accuracy of the algorithm; the specific results are shown in Figs. 5 and 6.

As can be seen in Fig. 5, the IGWO algorithm outperforms the other three compared algorithms in terms of overall search accuracy and convergence speed. From Fig. 5(a), (c), and (d), it can be seen that the IGWO algorithm, compared with the other algorithms, has a larger rate of change of the curves during the first 300 iterations, and the convergence speed is significantly faster than that of the other algorithms, which indicates that the IGWO algorithm possesses a stronger ability to search globally in the early stages. And from Figure Fig. 5(b), although the convergence speed advantage of IGWO is not very obvious compared with WOA algorithm, its final convergence accuracy is higher, indicating that IGWO has better optimization ability in the local search stage. Therefore, in summary, the IGWO algorithm shows a strong advantage in both convergence speed optimization and stability optimization.

From Fig. 6(a), (b), (c), and (d), it can be seen that the IGWO algorithm, compared with other algorithms, has a larger rate of change of the curve in the first 200 iterations, and the convergence speed is significantly faster than other algorithms.

TABLE VIII
SYSTEM PARAMETER

Parameters	Numerical values
Dc side voltage V_{dc}	380 V
Dc capacitance C_{dc}	470 μF
Filter inductance L_1	3 mH
Inductance L_1 internal resistance R_1	0.2 Ω
Filter capacitance C	1 μF
Capacitance C internal resistance R_c	0.015 Ω
Filter inductance L_2	0.94 mH
Inductance L_2 internal resistance R_2	0.1 Ω
Grid-connected voltage v_g	311 V
Switching frequency f_s	20 kHz
Weight coefficient a	0.5
Weight coefficient b	0.25
Weight coefficient c	0.25

In order to verify the effectiveness of the proposed IGWO algorithm in optimizing the weight coefficients method in MOMPC, MATLAB/Simulink is used for simulation. The system parameters are shown in Table VIII.

The maximum number of iterations is 100, and the fitness value of each algorithm is calculated. The system parameters are the same as those shown in Table VIII. The simulation results are shown in Fig. 7. It can be seen from Fig. 7 that IGWO achieves faster convergence with fewer iterations and improved convergence accuracy compared to the other algorithms.

Fig. 8 gives the number of switches and the THD values corresponding to the value λ solved by the IGWO algorithm. As can be seen in Fig. 8, the cost function corrected by the IGWO algorithm makes the current THD value of the inverter smaller and ensures that the current THD is as small as possible

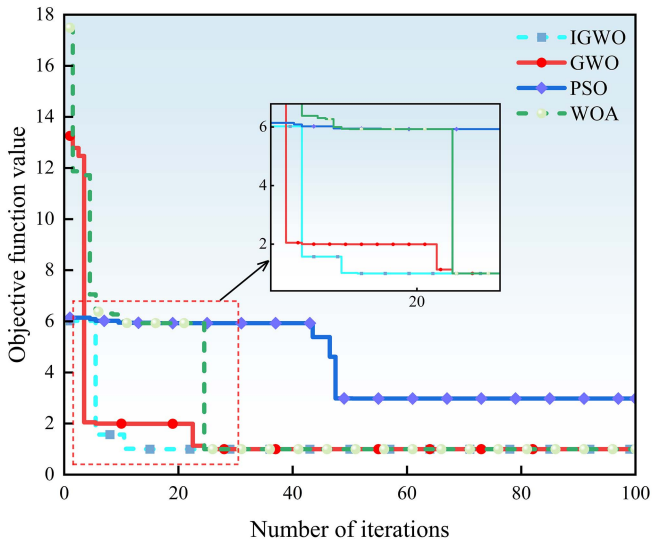

Fig. 7. Convergence curves.

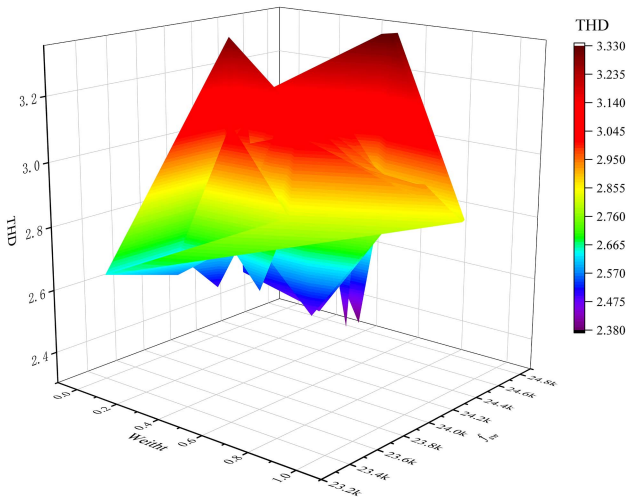

Fig. 8. Relationship between weighting factors λ and THD.

and has a small number of switches, and the current error of the objective function is as small as possible. The optimal value of the MOMPC after optimization by the IGWO algorithm is the value in the blue region, and the worse value is the value in the red region.

V. Experimental Results

In this section, the experimental results of the developed grid-connected system were provided. To validate the effectiveness of the IGWO algorithm in optimizing the weighting coefficients for MOMPC, an experimental platform is developed and tested using the implementation of DSP hardware.

Fig. 9 shows the block diagram of the hardware setup, which is mainly composed of the main power circuit and the control circuit. The main power circuit consists mainly of a dc power supply, a fuse, a single-phase full-bridge inverter based on the Infineon IGBT IGP20N65H5 module, an LCL-type filter, a relay, a load, and an ac power source. The control circuit includes current and voltage sensors to measure the actual current and voltage values, and a TMS320F28379D microcontroller for real-time control, signal processing, and driving the switching devices. To acquire and analyze signals, the Tektronix MDO4104 mixed domain oscilloscope is used, enabling precise monitoring of system performance.

A. System Startup

Before starting the system, it is essential to check the hardware and take the necessary precautions. Ensure that all wiring connections are correct, the fuses are intact, the inverter switch tube and relay are OFF, and the voltage and current sampling are functioning correctly. Initially, set the ac voltage of the power supply connected to the inverter output to 20 V, 50 Hz, which will provide current to the resistive load. After closing the relay, set the reference power and reactive power, then adjust to raise the dc bus voltage to 380 V and increase the ac output voltage to 220 V. Before enabling connection to the grid, ensure that the PLL successfully tracks the voltage phase of the grid to maintain synchronization. Finally, observe and verify the output voltage and current on both sides of the inverter to confirm stable operation. The experimental results are shown in Fig. 11. During the inverter's grid connection process, the phase difference between the inverter output voltage and the grid voltage causes the grid to absorb energy from the inverter. After 130 ms, the inverter completes phase tracking and successfully synchronizes with the grid.

B. Steady State Experiments

In order to verify the control performance of the IGWO-MOMPC algorithm in the grid-connected steady state, a steady state experiment was conducted on the system according to Fig. 2. The experimental platform is shown in Fig. 10. The input side voltage is set to 380 V, the active power is set to 250 W, the specific parameters are shown in Table VIII, and the experimental results are shown in Fig. 12.

The experimental results show that all three control strategies are able to maintain better current waveforms with a higher sinusoidality of the output current. Fig. 12(a) shows the output voltage and current waveforms under the PI control strategy and the THD is 4.50%, Fig. 12(b) presents the output current waveform under the MOMPC algorithm, where the THD with a weight coefficient of 1 is reduced to 3.96%. Further optimization using the IGWO algorithm, with an optimized weight coefficient of 0.12, reduces the THD of the inverter output current to 3.46%, as shown in Fig. 12(c). Compared with the PI algorithm and the MOMPC algorithm, the output current THD is significantly reduced, indicating that the IGWO-MOMPC is capable of optimizing the current tracking performance while effectively suppressing the harmonics and improving the steady-state control capability of the system.

C. Dynamic Experiments

To evaluate the dynamic performance of the IGWO-MOMPC algorithm in the grid-connected mode, experiments were carried out on the inverter to evaluate its performance under sudden

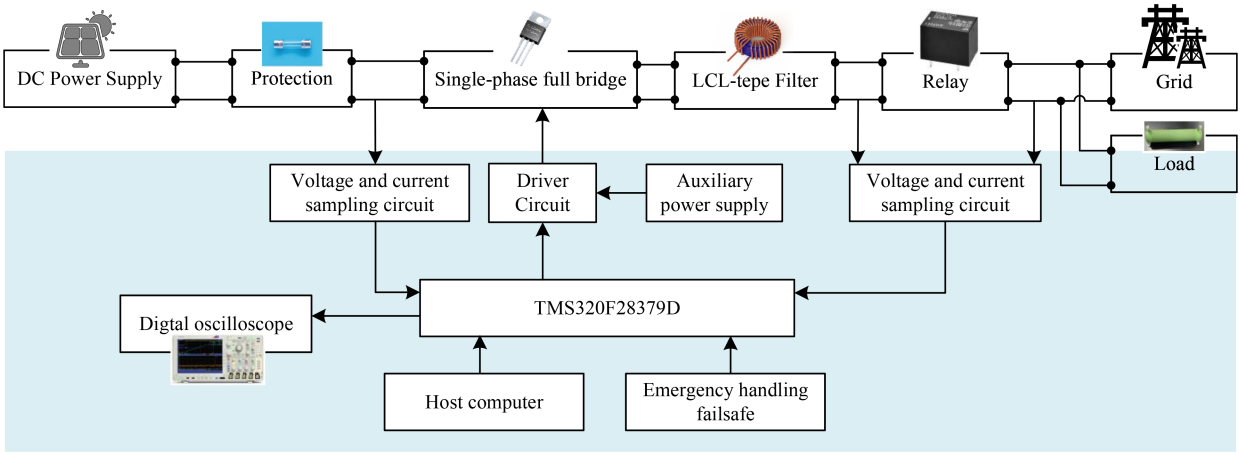

Fig. 9. Power and control diagram of the hardware setup.

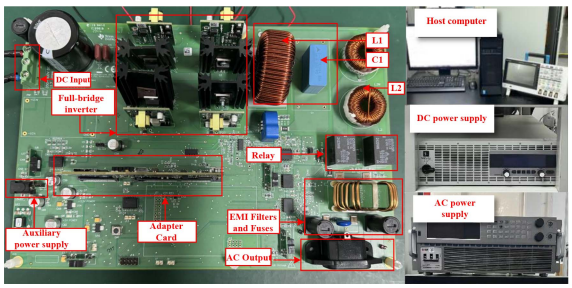

Fig. 10. Experimental platform.

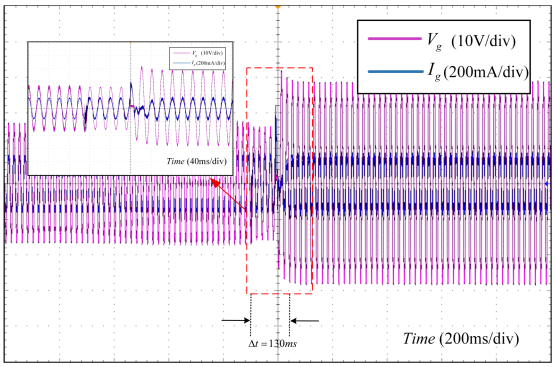

Fig. 11. Inverter system startup.

power changes and grid voltage sags. The input side voltage is set to 380 V and the active power is set to 250 W. The experimental results of sudden power changes are shown in Fig. 13, indicating that all three control strategies can effectively maintain stable voltage and current waveforms in grid-connected mode. When the reference power is increased to 300 W. The PI control strategy requires 110 ms to return to a steady state, as shown in Fig. 13(a). In comparison, the MOMPC algorithm restores the output current to a steady state within 72 ms, as illustrated in Fig. 13(b). In contrast, the regulation time of the IGWO-MOMPC algorithm is shortened to 47 ms to return to steady state, as shown in Fig. 13(c). Compared with the 110 ms regulation time of the PI algorithm, the regulation time is greatly reduced and the dynamic response speed is significantly improved. The experimental results show that the dynamic response speed is improved compared to MOMPC. Shows the superiority of the IGWO-MOMPC algorithm in sudden power change conditions, with a faster dynamic response capability.

TABLE IX
COMPARISON OF EXPERIMENTAL PERFORMANCE

Experimental condition	Control performance	PI	MOMPC	IGWO-MOMPC
Steady state	Current THD	4.50%	3.96%	3.46%
Grid-side active power change (250W→300W)	Dynamic response	110 ms	72 ms	47 ms
Grid voltage sag (220V→200V)	Dynamic response	80 ms	70 ms	62 ms

The experimental results of the grid voltage sag are shown in Fig. 14. When the voltage changes from 220 to 200 V, the PI control strategy requires 80 ms to return to a steady state, as shown in Fig. 14(a). In contrast, the MOMPC strategy returns to steady state in 70 ms, as illustrated in Fig. 14(b), showing a slight improvement over the PI control. However, the IGWO-MOMPC algorithm restores the system to steady state in just 62 ms, as shown in Fig. 14(c), demonstrating its superior dynamic response. These results highlight that the IGWO-MOMPC algorithm outperforms both the PI and the MOMPC strategies in terms of response speed, showing a clear advantage in handling voltage disturbances.

Table IX presents a detailed summary of the experimental results of the inverter under various operating conditions, including transient disturbances and load variations. The results demonstrate that the IGWO-MOMPC method significantly outperforms conventional control strategies in both dynamic and steady-state performance. In particular, the IGWO-MOMPC method not only ensures faster response times and improved voltage and current waveform stability but also exhibits enhanced robustness against disturbances, such as sudden power changes and grid voltage sags. These performance

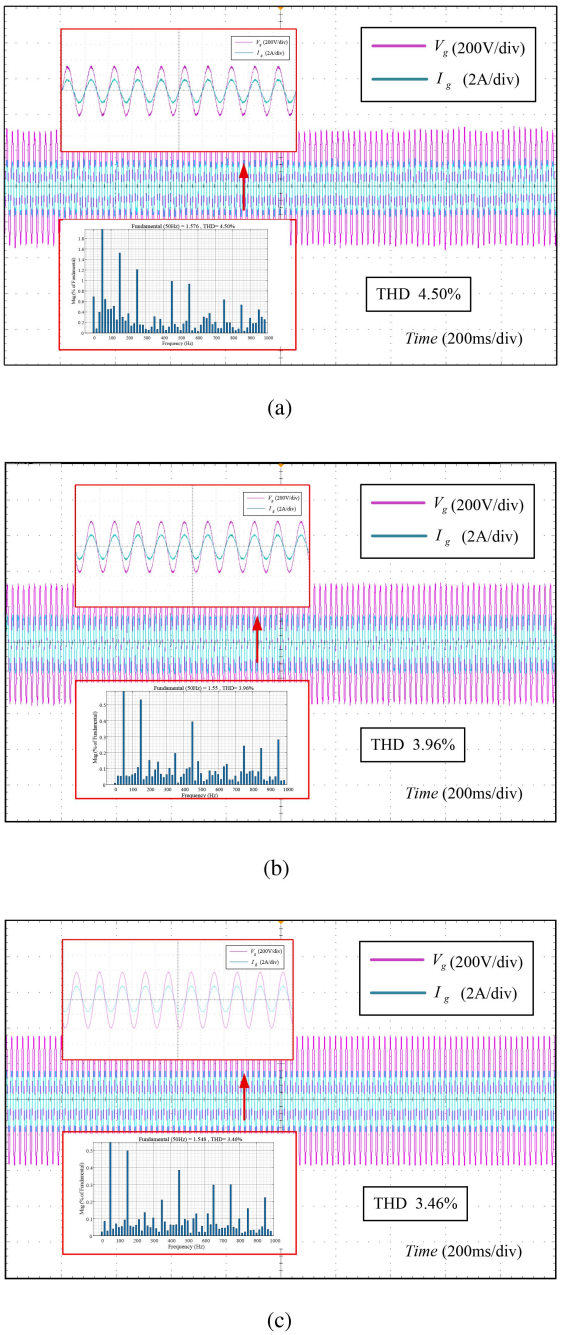

Fig. 12. Comparison experiments under steady-state. (a) PI. (b) MOMPC. (c) IGWO-MOMPC.

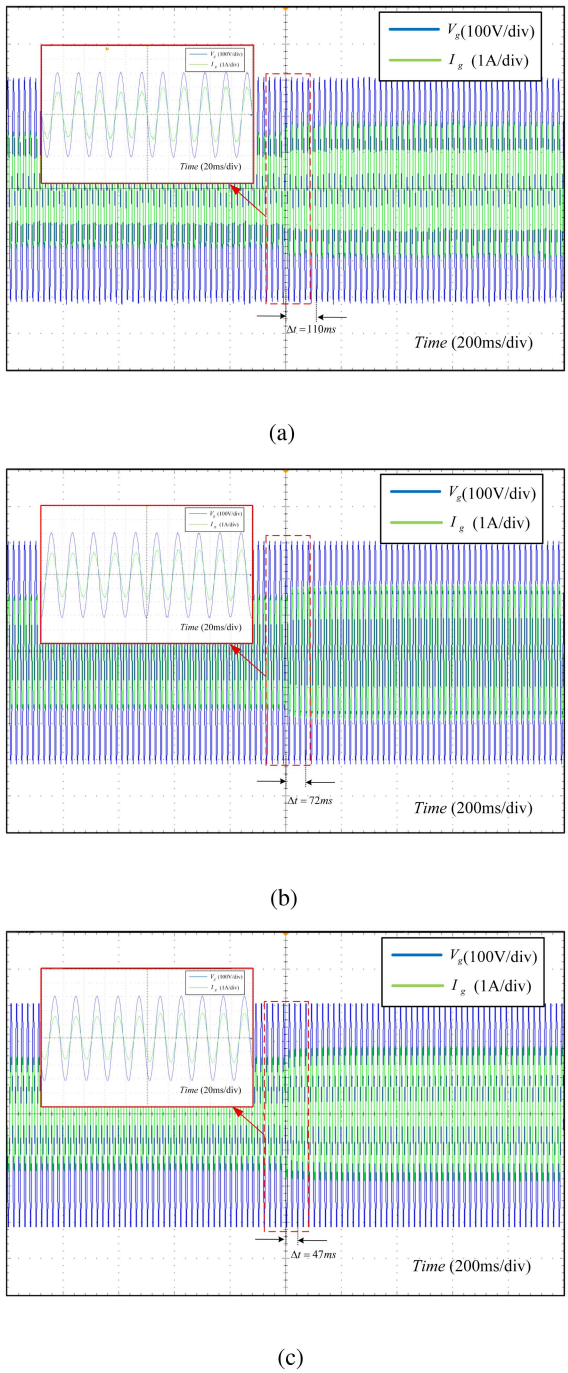

Fig. 13. Comparison experiments under sudden power change. (a) PI. (b) MOMPC. (c) IGWO-MOMPC.

improvements highlight the effectiveness of the proposed control strategy in real-world operating scenarios, where both the stability and efficiency of the system are critical.

The system efficiency of the inverter under different current conditions is shown in Fig. 15. The results indicate that, under the MOMPC control strategy, the system efficiency remains above 91.6% in all cases. At a current of 0.5 A, IGWO-MOMPC achieves an optimal system efficiency of 92.14% when $\lambda = 0.15$, while the efficiency under MOMPC is 91.7%, and the PI controller reaches only 90.8%. Furthermore, as the current increases, the overall efficiency of the system exhibits an upward trend. Specifically, at a current of 1 A, the optimal efficiency of IGWO-MOMPC reaches 93.1%, and at 1.5 A, it attains a maximum of 93.5%. These findings demonstrate that, under all current conditions, the IGWO-MOMPC control strategy consistently achieves superior system efficiency compared to MOMPC and PI control.

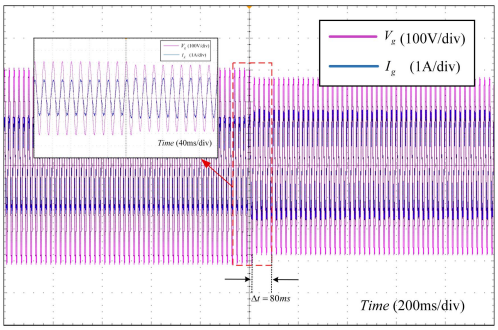

(a)

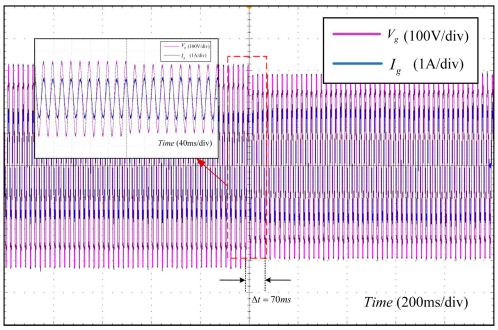

(b)

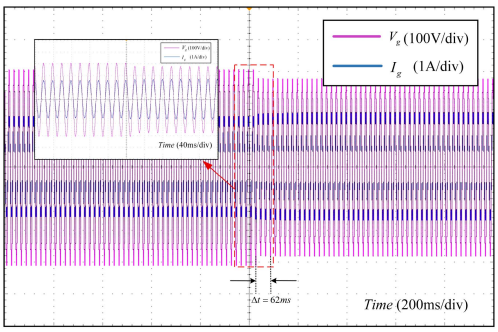

(c)

Fig. 14. Comparison experiments under grid voltage sag. (a) PI. (b) MOMPC. (c) IGWO-MOMPC.

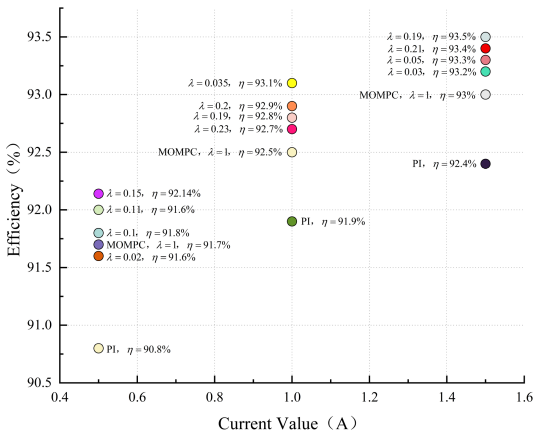

Fig. 15. Efficiency optimization comparison.

VI. Conclusion

In this article, an MOMPC strategy based on the IGWO algorithm is proposed for the LCL grid-connected inverters. The MOMPC weighting coefficients are optimized offline using the IGWO algorithm to balance current error, total harmonic distortion, and switching frequency. Compared to traditional MPC methods and other optimization algorithms, the proposed strategy demonstrates faster convergence speed, higher optimization accuracy, and superior dynamic response performance.

The IGWO algorithm effectively optimizes the weight coefficients in the MOMPC framework, addressing the challenges associated with multiobjective tradeoffs, such as minimizing THD, reducing current errors, and improving dynamic response performance. By integrating IGWO into the MOMPC framework, the system parameters including current error, THD, and switching frequency are effectively optimized. This ensures precise regulation of the inverter's output current and significantly enhances overall current quality. Furthermore, the multiobjective optimization approach guarantees that the inverter can more efficiently and accurately meet grid connection requirements. Theoretical analysis demonstrates that the IGWO-MOMPC strategy exhibits robust stability and adaptability under varying operating conditions, such as sudden power changes and grid voltage sags. The experimental results further validate the efficacy and practical applicability of the proposed algorithm.

References

[1] D. Pan, X. Ruan, C. Bao, W. Li, and X. Wang, "Optimized controller design for LCL-type grid-connected inverter to achieve high robustness against grid-impedance variation," *IEEE Trans. Ind. Electron.*, vol. 62, no. 3, pp. 1537–1547, Mar. 2015.

[2] K. Kim, H. Cha, and H.-G. Kim, "A new single-phase switched-coupled-inductor DC–AC inverter for photovoltaic systems," *IEEE Trans. Power Electron.*, vol. 32, no. 7, pp. 5016–5022, Jul. 2017.

[3] M. G. Judewicz, S. A. González, J. R. Fischer, J. F. Martínez, and D. O. Carrica, "Inverter-side current control of grid-connected voltage source inverters with LCL filter based on generalized predictive control," *IEEE J. Emerg. Sel. Topics Power Electron.*, vol. 6, no. 4, pp. 1732–1743, Dec. 2018.

[4] L. Zhou and M. Preindl, "Decentralized circulating current attenuation with model predictive control for distributed/shunted single/three-phase grid-tied inverters," *IEEE Trans. Power Electron.*, vol. 37, no. 10, pp. 11534–11539, Oct. 2022.

[5] J. Lei, S. Feng, P. Wheeler, B. Zhou, and J. Zhao, "Steady-state error suppression and simplified implementation of direct source current control for matrix converter with model predictive control," *IEEE Trans. Power Electron.*, vol. 35, no. 3, pp. 3183–3194, Mar. 2020.

[6] J. Rodriguez et al., "State of the art of finite control set model predictive control in power electronics," *IEEE Trans. Ind. Electron*, vol. 9, no. 2, pp. 1003–1016, May 2013.

[7] R. Rajamony, S. Wang, R. Navaratne, and W. Ming, "Multi-objective design of single-phase differential buck inverters with active power decoupling," *IEEE Open J. Power Electron.*, vol. 3, pp. 105–114, 2022.

[8] F. Wang, S. Li, X. Mei, W. Xie, J. Rodríguez, and R. M. Kennel, "Model-based predictive direct control strategies for electrical drives: An experimental evaluation of PTC and PCC methods," *IEEE Trans. Ind. Electron*, vol. 11, no. 3, pp. 671–681, Jun. 2015.

[9] D. Prajapati, A. Dekka, D. Ronanki, and J. Rodriguez, "Low-complexity Heun's method-based FCS-MPC with reduced common-mode voltage for a five-level inverter," *IEEE Trans. Power Electron.*, vol. 39, no. 3, pp. 3329–3338, Mar. 2024.

[10] Y. Han, C. Gong, L. Yan, H. Wen, Y. Wang, and K. Shen, "Multiobjective finite control set model predictive control using novel delay compensation technique for PMSM," *IEEE Trans. Power Electron.*, vol. 35, no. 10, pp. 11193–11204, Oct. 2020.
[11] Z. Ke et al., "Fractional-order model predictive control with adaptive parameters for power converter," *IEEE J. Emerg. Sel. Topics Power Electron.*, vol. 11, no. 3, pp. 2650–2660, Jun. 2023.
[12] J. Hu, J. Zhu, G. Lei, G. Platt, and D. G. Dorrell, "Multi-objective model-predictive control for high-power converters," *IEEE Trans. Energy Convers.*, vol. 28, no. 3, pp. 652–663, Sep. 2013.
[13] E. Zerdali, M. Rivera, and P. Wheeler, "A review on weighting factor design of finite control set model predictive control strategies for AC electric drives," *IEEE Trans. Power Electron.*, vol. 39, no. 8, pp. 9967–9981, Aug. 2024.
[14] X. G. Zhang and Y. K. He, "Direct voltage-selection based model predictive direct speed control for PMSM drives without weighting factor," *IEEE Trans. Power Electron.*, vol. 34, no. 8, pp. 7838–7851, Aug. 2019.
[15] P. Cortes et al., "Guidelines for weighting factors design in model predictive control of power converters and drives," in *Proc. IEEE Int. Conf. Ind. Technol.*, Churchill, VIC, Australia, 2009, pp. 1–7.
[16] F. X. Wang et al., "Design of model predictive control weighting factors for PMSM using Gaussian distribution-based particle swarm optimization," *IEEE Trans. Ind. Electron*, vol. 69, no. 11, pp. 10935–10946, Nov. 2022.
[17] H. Fretes et al., "Pareto optimal weighting factor design of predictive current controller of a six-phase induction machine based on particle swarm optimization algorithm," *IEEE Trans. Emerg. Sel. Topics Power Electron.*, vol. 10, no. 1, pp. 207–219, Feb. 2022.
[18] Y. Gao, T. Yang, T. Dragičević, S. Bozhko, P. Wheeler, and C. Zheng, "Optimal filter design for power converters regulated by FCS-MPC in the MEA," *IEEE Trans. Power Electron.*, vol. 36, no. 3, pp. 3258–3268, Mar. 2021.
[19] P. R. U. Guazzelli, W. C. de Andrade Pereira, C. M. R. de Oliveira, A. G. de Castro, and M. L. de Aguiar, "Weighting factors optimization of predictive torque control of induction motor by multiobjective genetic algorithm," *IEEE Trans. Power Electron.*, vol. 34, no. 7, pp. 6628–6638, Jul. 2019.
[20] A. S. Soliman, M. M. Amin, F. F. M. El-Sousy, and O. A. Mohammad, "Experimental validation for artificial data-driven tracking control for enhanced three-phase grid-connected boost rectifier in DC microgrids," *IEEE Trans. Ind. Appl.*, vol. 59, no. 2, pp. 2563–2580, Mar./Apr. 2023.
[21] S. A. Davari, V. Nekoukar, C. Garcia, and J. Rodriguez, "Online weighting factor optimization by simplified simulated annealing for finite set predictive control," *IEEE Trans. Ind. Inform.*, vol. 17, no. 1, pp. 31–40, Jan. 2021.
[22] S. Mirjalili, S. M. Mirjalili, and A. Lewis, "Grey Wolf optimizer," *Adv. Eng. Softw.*, vol. 69, pp. 46–61, 2014.
[23] N. Guler and H. Komurcugil, "Energy function-based finite control set predictive control strategy for single-phase split source inverters," *IEEE Trans. Ind. Electron.*, vol. 69, no. 6, pp. 5669–5679, Jun. 2022.
[24] M. F. Umar et al., "Single-phase grid-interactive inverter with resonance suppression based on adaptive predictive control in weak grid condition," *IEEE J. Emerg. Sel. Topics Ind. Electron.*, vol. 3, no. 3, pp. 809–820, Jul. 2022.
[25] S. Vazquez et al., "An artificial intelligence approach for real-time tuning of weighting factors in FCS-MPC for power converters," *IEEE Trans. Ind. Electron*, vol. 69, no. 12, pp. 11987–11998, Dec. 2022.
[26] K. Balasubramanian, K. Ramya, and K. G. Devi, "Optimized adaptive neuro-fuzzy inference system based on hybrid grey wolf-bat algorithm for schizophrenia recognition from EEG signals," *Cogn. Neurodynamics*, vol. 17, no. 1, pp. 1–19, 2022.
[27] D. Guha, P. K. Roy, and S. Banerjee, "Load frequency control of large scale power system using quasi-oppositional Grey Wolf optimization algorithm," *Int. J. Eng. Sci. Technol.*, vol. 19, no. 4, pp. 1693–1713, 2016.
[28] R.-E. Precup, R.-C. David, and E. M. Petriu, "Grey wolf optimizer algorithm-based tuning of fuzzy control systems with reduced parametric sensitivity," *IEEE Trans. Ind. Electron.*, vol. 64, no. 1, pp. 527–534, Jan. 2017.
[29] K. C. and U. M. G., "Design of Gray Wolf optimizer algorithm-based fractional order PI controller for power factor correction in SMPS applications," *IEEE Trans. Power Electron.*, vol. 35, no. 2, pp. 2100–2118, Feb. 2020.

Fengxiang Wang (Senior Member, IEEE) was born in Jiujiang, China, in 1982. He received the B.S. degree in electronic engineering and the M.S. degree in automation from Nanchang Hangkong University, Nanchang, China, in 2005 and 2008, respectively, and the Ph.D. degree in electrical engineering from the Institute for Electrical Drive Systems and Power Electronics, Technische Universität München, Munich, Germany, in 2014.

He is currently a Full Professor and the Deputy Director with the Quanzhou Institute of Equipment Manufacturing, Haixi Institutes, Chinese Academy of Sciences, Beijing, China. His research interests include predictive control and sensorless control for electrical drives and power electronics.

Dr. Wang is an IET Fellow and an Associate Editor for IEEE TRANSACTIONS ON INDUSTRIAL ELECTRONICS and IEEE TRANSACTIONS ON ENERGY CONVERSION. As the General Chair, he organized IEEE 5th International Symposium on Predictive Control of Electrical Drives and Power Electronics (PRECEDE).

Feng Cai was born in Longyan, China, in 1998. He received the B.S. degree in information management and information system from Anhui Polytechnic University, Wuhu, China. He is currently working toward the master's degree in electronic information with Fujian Agriculture and Forestry University in collaboration with the Fujian Institute of Materials and Structures, Chinese Academy of Sciences, Beijing, China.

His research focuses on the predictive control of new energy power electronics.

Dongxiao Huang (Senior Member, IEEE) was born in Quanzhou, China, in 1987. He received the B.S. degree in biomedical engineering and the M.S. degree in instrument engineering from Tianjin University, Tianjin, China, in 2011 and 2015, respectively.

He is currently with Haixi Institutes, Chinese Academy of Sciences, Beijing, China. His research interests include wireless power transmission and predictive control for power converter.

Yao Wei (Member, IEEE) was born in Handan, China, in 1993. He received the B.S. and Ph.D. degrees in power electronics and power transmission from Yanshan University, Qinhuangdao, China, in 2015 and 2021, respectively.

Since 2021 to 2024, he was a Postdoctoral with the Quanzhou Institute of Equipment Manufacturing, Haixi Institutes, Chinese Academy of Sciences, Jinjiang, China, where he is currently an Assistant Researcher. His research interests include driving and advanced control for electric vehicles and servosystems.

Dr. Wei is a Senior Member of China Electrotechnical Society (CES) and Member of Chinese Society for Electrical Engineering (CSEE).

Dongliang Ke (Senior Member, IEEE) was born in Quanzhou, China, in 1986. He received the B.S. degree in electrical engineering and the M.S. degree in power electronics and power drives from Northwestern Polytechnical University, Xi'an, China, in 2010 and 2013, respectively.

He is currently a Postdoctoral Supervisor, Deputy Director of the Electrical Drives Laboratory and Senior Engineer of Quanzhou Institute of Equipment Manufacturing, Haixi Institutes, Chinese Academy of Sciences, Beijing, China. His research interests include predictive control, flux-oriented control, sensorless control and identification for electrical drives and power converters.

Dr. Ke is an IET Member, and Member of the Chinese Society for Electrical Engineering. He was also a Session Chair of the IEEE 5th International Symposium on Predictive Control of Electrical Drives and Power Electronics (PRECEDE).

Zhenbin Zhang (Senior Member, IEEE) was born in Shandong, China, in 1984. He received the Ph.D. (*summa cum laude*) degree in electrical and energy engineering from the Technical University of Munich, Munich, Germany, in 2016.

He was a Postdoctoral in electrical and energy engineering with the Technical University of Munich. Since 2017, he has been a Full Professor with Shandong University, Jinan, China, where he is currently the Director for both the Laboratory of More Power Electronics Energy Systems and the Institute of Sustainable Energy and Smart Grids. His research interests include power electronics and electrical drives, sustainable energy system, smartgrids, and microgrids.

Dr. Zhang was the recipient for VDE Award-2017 in Suedbayern, Germany, and an Associate Editor for IEEE TRANSACTIONS POWER ELECTRON. He is currently an IET Fellow Member and IET Chartered Engineer.